PERGAMON

International Journal of Heat and Mass Transfer 44 (2001) 4445–4454

International Journal of HEAT and MASS TRANSFER

www.elsevier.com/locate/ijhmt

Heat and mass transfer coefficients of viscous spheres

Zhi-Gang Feng, Efstathios E. Michaelides *

School of Engineering and Center for Bioenvironmental Research, Tulane University, New Orleans, LA 70118, USA

Received 17 May 2000; received in revised form 28 February 2001

Abstract

The problem of mass/heat transfer from a viscous droplet is solved by using a finite-difference scheme, and a dual kind of computational grid. The steady-state Navier–Stokes and energy equations for the flow fields inside and outside a viscous sphere in a fluid of different properties are fully solved numerically for Reynolds numbers (*Re*) ranging from 1 to 500. The corresponding Peclet numbers (*Pe*) range from 1 to 1000. At high values of *Re* and *Pe* a thermal and a momentum boundary layer are formed in the outside fluid. For this reason, we adopted a method of a two sub-layer concept for the computational domain outside the sphere. The first of these computational sub-layers is positioned at the interface of the sphere and covers a thin region [of $O(Re^{-1/2})$ for the momentum and of $O(Pe^{-1/2})$ for the thermal boundary layer]. The second computational layer is based on an exponential function and covers the rest of the domain. We utilize this numerical technique to compute the Nusselt numbers for viscous spheres at different values of *Re*, *Pe* and the viscosity ratio. The computations also show that the effect of the internal fluid density on the heat or mass transfer is negligible.

1. Introduction

The problem of momentum or heat/mass transfer from a sphere is one of the most fundamental problems in transport processes. Practical processes, such as the heat or mass transfer from bubbles rising in a liquid or from drops moving in a fluid of different properties, combustion processes and chemical reactions involving fluids, are some of the applications of this subject. Because of the many practical applications and the scientific interest it generates, the subject has been studied extensively, starting with the pioneering work of Fourier [1], which applies to a rigid sphere. Some of the more recent work on the subject includes the treatises and monographs by Levich [2], Soo [3], Clift et al. [4], Leal [5] and Sirignano [6].

Friedlander [7] was the first to determine asymptotically the Sherwood number for a small rigid sphere and for large *Pe* by applying the boundary-layer theory and assuming a concentration profile with coefficients derived from the boundary conditions. Acrivos and Taylor [8] also used an asymptotic method and applied their study to a Stokesian velocity field, which implies very small *Re*. They discussed the effect of small but finite *Re* of the rigid sphere when *Pe* is large and, derived another asymptotic expression for the Sherwood number (always at large *Pe*).

Among the studies on the heat transfer from a solid sphere one must mention a numerical study by Abramzon and Elata [9] who computed the transient heat transfer coefficient for rigid spheres assuming a Stokesian velocity field (which implies low *Re*) outside the sphere. In another numerical study, Feng and Michaelides [10] relaxed the Stokesian velocity field assumption and used the full Navier–Stokes equations to compute numerically the velocity and temperature fields around a solid sphere. Hence, they derived transient and steady-state heat transfer coefficients at high *Re* and *Pe*. The same authors [11] also used a numerical method to compute the effect of the viscosity ratio and of *Pe* on the Sherwood number of a viscous sphere under creeping flow conditions (Stokesian velocity field). Among the computational studies on this subject one must mention the ones by Haywood et al. [12] who computed the transport properties of evaporating droplets and the one by Chiang et al. [13] who computed the transient heat

* Corresponding author. Tel.: +1-504-865-5764; fax: +1-504-862-8747.

E-mail address: emichael@tulane.edu (E.E. Michaelides).

0017-9310/01/$ - see front matter
PII: S0017-9310(01)00090-4

Nomenclature

a	radius of the sphere
Bo	Bond number
c	specific heat capacity
D	heat or mass diffusivity
d	diameter of the sphere ($=2a$)
E	operator defined in (7)
g	gravitational acceleration
k	thermal conductivity
Nu	Nusselt number
r	radial direction
Pe	Peclet number
Pr	Prandtl number
Re	Reynolds number
Sc	Schmidt number
U	average velocity
x, y	coordinates in the stretched computational domain
Y_E	y coordinate corresponding to the edge of external domain

Greek symbols

ζ	function related to the vorticity
θ	azimuthal coordinate
Θ	temperature/concentration
κ	density ratio
λ	viscosity ratio
μ	dynamic viscosity
ρ	density
Ψ	stream function
Ω	vector related to the vorticity function

Subscripts

i	pertains to the internal flow
o	pertains to the external flow
s	pertains to the surface of the sphere
∞	pertains to conditions far from the sphere

Superscript

$'$	(prime) denotes dimensional quantities

transfer from evaporating droplets at various initial temperatures for moderate values of Re.

It is well known that the process of heat or mass convection from a fluid–fluid interface differs significantly from that at a fluid–solid body interface, because of the induced fluid motion on both sides of the interface. Early experiments by Hammerton and Garner [14] performed at relatively high Re showed that the rate of mass transfer increases significantly from circulating bubbles of slightly soluble pure gases, compared to bubbles where no appreciable circulation takes place. This observation has been subsequently confirmed for many other types of viscous spheres [4].

Feng and Michaelides [15] derived an asymptotic solution for the case of transient mass or heat transfer from a droplet at low but finite Pe ($Pe < 1$). They showed that the effect of the circulation (and of Pe) is not significant when Pe is small. However, this is not the case for large Pe. Assuming a Stokesian flow, Bowman et al. [16] computed the effect of the circulation inside the fluid sphere on the mass and heat transfer rate at high Pe and found that the internal circulation and advection of the fluid may increase the rate of heat or mass transfer by as much as 100%. Levich [2] also showed the importance of the internal circulation and provided an analytical first-order solution for the same problem, which is applicable to low values of the viscosity ratio.

In this study, we employ a finite-difference scheme to solve the full Navier–Stokes equations for both the external and the internal flow fields of the sphere, for Reynolds numbers in the range 0–500. Hence, the heat/mass transfer equation is solved and the Nusselt/Sherwood numbers are obtained under the condition of constant temperature/concentration at the fluid-to-fluid interface. The range of the results covers all possible values of the viscosity ratio, Pe up to 1000, and Re up to 500. The results are presented in a tabular form and in the form of a correlation, which may become very useful in engineering calculations.

2. Governing equations and boundary conditions

We consider a fluid sphere (a bubble or a drop) with density ρ_i and viscosity μ_i, which translates rectilinearly in a continuous fluid of density ρ_o and viscosity μ_o. The undisturbed fluid velocity with respect to the center of the sphere is U_∞. All properties of the sphere will be denoted by the subscript i, while those of the outer fluid will be denoted by the subscript o. The coordinate system is chosen to be spherical with its origin fixed at the center of the droplet and with $\theta = 0$ in the downstream direction.

We use the following dimensionless variables for the radial distance, the stream function, the vorticity, and the temperature:

$$r = \frac{r'}{a}, \quad \Psi = \frac{\Psi'}{U_\infty a^2}, \quad \Omega = \frac{\Omega' a}{U_\infty}, \quad \Theta = \frac{\Theta' - \Theta'_\infty}{\Theta'_s - \Theta'_\infty}, \quad (1)$$

where the prime denotes dimensional variables and Ω' is a dimensional function related to the z component of the vorticity, ζ, by the following expression:

$$\Omega' = \zeta' r' \sin\theta. \tag{2}$$

Under these conditions, the dimensionless continuity and momentum equations for the internal flow field become

$$E^2 \Psi_i = \Omega_i, \tag{3}$$

and

$$\frac{Re_i}{2}\sin\theta\left[\frac{\partial}{\partial r}\left(\frac{\Omega_i}{r^2\sin^2\theta}\frac{\partial\Psi_i}{\partial\theta}\right) - \frac{\partial}{\partial\theta}\left(\frac{\Omega_i}{r^2\sin^2\theta}\frac{\partial\Psi_i}{\partial y}\right)\right] = E^2\Omega_i. \tag{4}$$

We also consider a stretched coordinate system for the external flow field given by the transformation $r = \exp(y)$ or $y = \ln r$. Hence, the corresponding governing equations for the external flow field become

$$E^2 \Psi_o = \Omega_o, \tag{5}$$

and

$$\frac{Re}{2}e^{y}\sin\theta\left[\frac{\partial}{\partial y}\left(\frac{\Omega_o}{e^{2y}\sin^2\theta}\frac{\partial\Psi_o}{\partial\theta}\right) - \frac{\partial}{\partial\theta}\left(\frac{\Omega_o}{e^{2y}\sin^2\theta}\frac{\partial\Psi_o}{\partial y}\right)\right] = e^{2y}E^2\Omega_o. \tag{6}$$

The operator E^2 is defined as follows:

$$E^2 = \frac{\partial^2}{\partial r^2} + \frac{\sin\theta}{r^2}\frac{\partial}{\partial\theta}\left(\frac{1}{\sin}\frac{\partial}{\partial\theta}\right). \tag{7}$$

The dimensionless steady-state energy or mass transfer equation for the fluid may be written as follows:

$$\frac{Pe}{2}\left[\frac{\partial\Psi_o}{\partial y}\frac{\partial}{\partial\theta}\left(\frac{\Theta}{e^{2y}\sin\theta}\right) - \frac{\partial\Psi_o}{\partial\theta}\frac{\partial}{\partial y}\left(\frac{\Theta}{e^{2y}\sin\theta}\right)\right] = e^{2y}E^2\Theta. \tag{8}$$

In this problem we assume that the surface of the sphere has constant temperature or material concentration denoted by the variable Θ'_S. We also assume that the ambient fluid temperature/concentration is denoted by Θ'_∞. The dimensionless temperature concentration in the two flow fields is given in (1). The Reynolds and Peclet numbers, which appear in the previous expressions are given as follows:

$$Re_i = \frac{2\rho_i a U_\infty}{\mu_i}, \quad Re = \frac{2\rho_o a U_\infty}{\mu_o} \quad \text{and} \quad Pe = \frac{2aU_\infty}{D_o}. \tag{9}$$

Since most of the boundary conditions pertain to the fluid–fluid interface, for clarity, the interface will be denoted as $r = 1$ when it is approached from inside and as $y = 0$ when it is approached from the outside flow field. The boundary conditions for the stream function and the vorticity may be written as follows:

A. At the center of the viscous sphere:

$$\Psi_i = 0, \quad \Omega_i = 0 \quad \text{at } r = 0. \tag{10}$$

B. At the fluid–fluid interface,

$$\Psi_i = 0, \quad \Psi_o = 0 \quad \text{at } r = 1 \text{ or } y = 0. \tag{11}$$

C. The balance of forces in the tangential direction at the fluid–fluid interface also yields:

$$\lambda\left(\frac{\partial^2\Psi_i}{\partial r^2} - 2\frac{\partial\Psi_i}{\partial r}\right)_{r=1} = \left(\frac{\partial^2\Psi_o}{\partial y^2} - 3\frac{\partial\Psi_o}{\partial y}\right)_{y=0}. \tag{12}$$

D. The conservation of mass in the tangential direction at the interface results in the following expression:

$$\left.\frac{\partial\Psi_i}{\partial r}\right|_{r=1} = \left.\frac{\partial\Psi_o}{\partial y}\right|_{y=0}. \tag{13}$$

E. Far from the center of the droplet, at the distance $y = Y_E$, or $r = \exp(Y_E)$, the flow is undisturbed and unidirectional. Hence, the values of the functions Ψ and Ω are:

$$\Psi_o = \frac{1}{2}e^{2y}\sin^2\theta, \tag{14}$$

$$\Omega_o = 0. \tag{15}$$

Since, there are no explicit conditions for the functions Ω_i and Ω_o, we evaluate these functions at the interface from their relationship to the stream function:

$$\Omega_i = \left.\frac{\partial^2\Psi_i}{\partial r^2}\right|_{r=1}, \quad \Omega_o = \left.\left(\frac{\partial^2\Psi_o}{\partial y^2} - \frac{\partial\Psi_o}{\partial y}\right)\right|_{y=0}. \tag{16}$$

F. Finally, for the mass or heat transfer equation, the pertinent boundary conditions are

$$\Theta = 1 \quad \text{at } y = 0, \quad \text{and} \quad \Theta \to 0 \quad \text{as } y = Y_E. \tag{17}$$

3. Numerical implementation

When $Re > 100$ or $Pe > 100$, a momentum or a thermal boundary layer (or both) will be formed at the interface of the sphere. The thickness of these boundary layers is of the order of $O(Re^{-1/2})$ and $O(Pe^{-1/2})$ respectively. It appears that the exponential grid, which was used in previous studies on droplet behavior [18,19], is not adequate to capture the details of momentum and heat transfer in these boundary layers, especially at small values of the viscosity ratio, λ. For this reason, we are using a different approach, whose basic premise is to separate the computational domain for the external field, into two separate sub-domains:

- The first sub-domain is very dense and covers the region of the two boundary layers.
- The second sub-domain is exponential and includes the remaining of the flow domain.

For example, in the case of $Re = 100$ and $Pe = 500$, we have chosen as the first sub-domain the region $0.00 < y < 0.05$ and have placed 50 uniformly spaced grid points, thus achieving a mesh size equal to 0.001 of the sphere radius. For the outside sub-domain, we have used a mesh of another 150 grid points. In order to achieve a smooth transition, the interface region of the two sub-domains is non-uniform.

It must be pointed out that, at high Re, a thin boundary layer is also formed inside the sphere. However, the external flow velocity field is not sensitive to this boundary layer [17]. This is also corroborated by the fact that the density ratio (which is related to the internal Re) does not affect the heat transfer rate, as shown in Section 4.5.

The force on the sphere depends on the normal derivative of the vorticity function, Ω_o, and the latter on the higher derivatives of the stream function Ψ_o [17,18]. Therefore, high accuracy for the stream function is required near the interface. In order to achieve the required degree of accuracy, we use two cubic polynomials for the interpolation of the stream function between nearby points on either side of the interface (three rows of grid points in either direction). Thus, the stream function expressions in the vicinity of the fluid-to-fluid interface become

$$\Psi_i = ay^3 + by^2 + cy + d \tag{18a}$$

for the internal flow, and

$$\Psi_o = A(1-r)^3 + B(1-r)^2 + C(1-r) + D \tag{18b}$$

for the external flow.

Using the boundary conditions given in Section 2, the coefficients a, b, c, d and A, B, C may be obtained in terms of the stream function at all the grid points. In the case of uniformly distributed grid points, we obtain the following expressions for the vorticity function:

$$\Omega_{i,Ni} = \frac{-7\Psi_{i,Ni} + 8\Psi_{i,Ni-1} - \Psi_{i,Ni-2} + 6c\Delta r}{2\Delta r^2}, \tag{19}$$

and

$$\Omega_{o,0} = \frac{-7\Psi_{o,0} + 8\Psi_{o,1} - \Psi_{o,2} - 6c\Delta y}{2\Delta y^2} - c, \tag{20}$$

where c is given by the following expression:

$$\begin{aligned} c = \{&\lambda(-7\Psi_{i,Ni} + 8\Psi_{i,Ni-1} - \Psi_{i,Ni-2})\Delta y^2 \\ &- (-7\Psi_{o,0} + 8\Psi_{o,1} - \Psi_{o,2})\Delta r^2\}/\{2\Delta r\Delta y \\ &\times [(2\lambda - 3)\Delta r\Delta y - 3(\lambda\Delta y + \Delta r)]\}. \end{aligned} \tag{21}$$

For the computations presented in this paper, the value $y_E = 5$ (or equivalently, $r_\infty = 148.4$) is used. A grid of 180 points has been used in the radial direction (with 50 points reserved for the boundary layer sub-domain as mentioned above). The number of points in the traverse direction varied with Re or Pe and is at least 180. For the domain inside the sphere, a grid sensitivity analysis revealed that 80 grid points in the radial direction are sufficient for the high viscosity ratio cases, where the velocities are lower, (that is, $\lambda > 1$), while fewer grid points (as low as 60) are sufficient for the lower values of λ. It must be pointed out that we have conducted grid validation calculations by using finer grids with two to three times as many points for both the inside and the outside domains and found that the solutions obtained were always within 1% of those obtained by the coarser grid. This gave us an indication that the grids used are satisfactory for the required computations. The comparisons of the results with asymptotic solutions, which are presented in Section 4.4, as well as the drag coefficient validations performed in [17], are additional indications of the accuracy of our computations.

The convergence criterion for the iterations is chosen, such that the largest relative fractional difference of any quantity, ϕ, between two consecutive iterations is less than 10^{-5}, i.e.,

$$\frac{|\phi^{(n+1)} - \phi^{(n)}|}{\max(|\phi^{(n)}|, 1)} \leqslant 10^{-5}. \tag{22}$$

From the computations it was found that large values of Re and Pe facilitate the faster convergence of the program.

4. Results and discussion

4.1. Flow field and temperature/concentration profile around a viscous sphere and results for Nu/Sh

Observations on the structure of the flow field and the streamlines showed that at low Re there is no recirculation flow at the downstream side of the sphere. However, when Re increases, a recirculation region is formed behind the viscous sphere and becomes very pronounced with the increase of Re. It is expected that this recirculation would facilitate the heat/mass transfer process. Similar observations on the corresponding results from the temperature/concentration equation, show that the concentration contours are closer together at higher Re, which would result in higher gradients and higher mass transfer. In the case of heat transfer, an analogous observation can be made: the rate of heat transfer increases with Re at constant Pe. This is demonstrated in the results of Fig. 1, which shows the local Nusselt numbers at different Re when $Pe = 100$ and the viscosity ratio is equal to 10.0. It is obvious that the local Nu/Sh increases with Re, except in a small region located

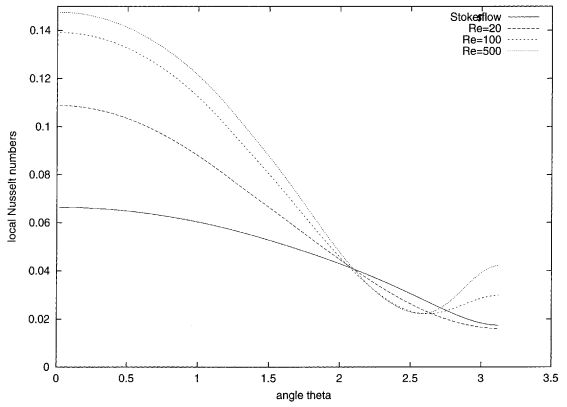

Fig. 1. Local Nusselt numbers at various Re when $Pe = 100$, $\lambda = 10.0$.

slightly above the recirculation region, where the local velocity and the local value of Re differ substantially from those shown in the legend of the figure.

Computations with the viscosity ratio as the parameter reveal that when the viscosity of the sphere is equal to that of the outside fluid, no recirculation occurs behind the sphere. When the internal fluid viscosity is much higher (ten times) the sphere behaves more like a solid sphere and flow recirculation downstream is evident. Computations on the Schmidt (or Prandtl) number show that, in the case of higher Sc or Pe, the concentration gradients near the sphere are substantially higher, which would indicate a higher rate of mass or heat transfer. This is demonstrated in Fig. 2, which shows the local Nusselt (or Sherwood) numbers when $Re = 200$ and $\lambda = 10$ for different Pe. It is obvious that higher Pr or Sc result in substantially higher values for Nu or Sh.

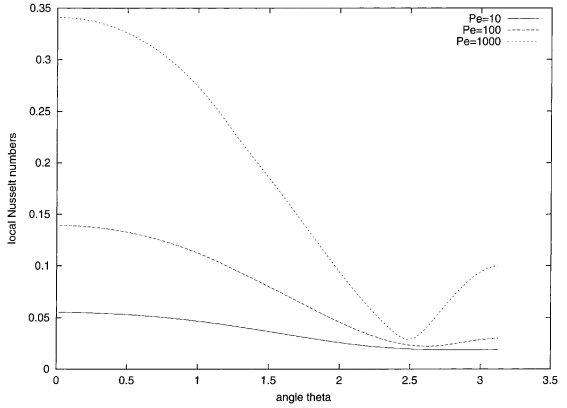

Fig. 2. Local Nusselt numbers at different Pe when $Re = 200$, $\sigma = 10$.

Fig. 3 depicts the local Nusselt/Sherwood numbers at various viscosity ratios when $Pe = 100$ and $Re = 200$. It is evident that the local Nu/Sh decreases with an increase in λ, everywhere except in the region behind the sphere where recirculation occurs. The area-average heat/mass transfer coefficient is lower with an increase of λ. This is in agreement with the fact that bubbles have higher overall heat transfer coefficients than solid spheres [4].

4.2. The drag coefficients of a viscous sphere

Using a similar numerical method, Feng and Michaelides [17] derived engineering correlations for the drag coefficients of a viscous sphere in the range $0 < Re < 1000$. These correlations are as follows:

$$C_D(Re,\lambda) = \frac{2-\lambda}{2} C_D(Re,0) + \frac{4\lambda}{6+\lambda} C_D(Re,2) \quad \text{for } 0 \leqslant \lambda \leqslant 2, \text{ and } 5 < Re \leqslant 1000, \tag{23a}$$

and

$$C_D(Re,\lambda) = \frac{4}{\lambda+2} C_D(Re,2) + \frac{\lambda-2}{\lambda+2} C_D(Re,\infty) \quad \text{for } 2 \leqslant \lambda \leqslant \infty, \text{ and } 5 < Re \leqslant 1000, \tag{23b}$$

where the functions $C_D(Re,0)$, $C_D(Re,2)$ and $C_D(Re,\infty)$ are the drag coefficients of spheres at $\lambda = 0$ (inviscid bubble), $\lambda = 2$, and $\lambda = \infty$ (solid sphere) respectively and are given by the following expressions:

$$C_D(Re,0) = \frac{48}{Re}\left(1 + \frac{2.21}{\sqrt{Re}} - \frac{2.14}{Re}\right), \tag{24a}$$

$$C_D(Re,2) = 17.0 Re^{-2/3}, \tag{24b}$$

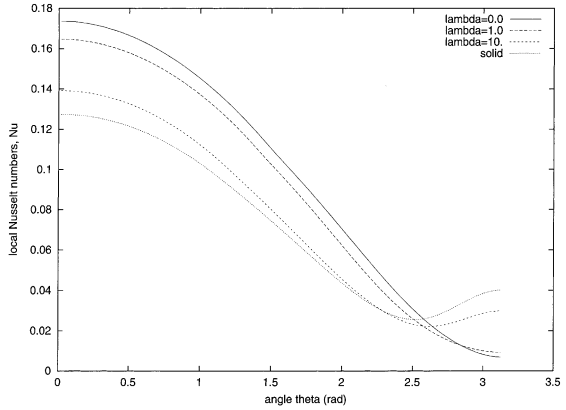

Fig. 3. Local Nusselt numbers for $Re = 200$, $Pe = 100$ with different viscosity ratio.

and

$$C_D(Re,\infty)=\frac{24}{Re}\left(1+\frac{1}{6}Re^{2/3}\right). \tag{24c}$$

4.3. Numerical results for the Nusselt/Sherwood numbers for a viscous sphere

The governing equations were solved to yield the rate of heat/mass transfer and, hence, the Nusselt/Sherwood numbers for a viscous sphere. The results are presented in Table 1 with Re, Pe and the viscosity ratio λ as parameters. It must be pointed out that the results for $Re\to 0$ have been derived by using the Stokes flow velocity profile around the sphere. In this case, the velocity field around the sphere was given by an analytic expression [5,6,11] and only the energy/mass transfer equation was solved numerically. The results for finite values of Re were derived by simultaneously solving the continuity, the momentum and the energy equations. Some other general conclusions that may be made from a glance at the results of Table 1 are that the Nusselt/Sherwood numbers increase with Pe (at constant Re) or with Re (at constant Pe) and decrease with λ.

From the results of Table 1, it is evident that for small Re ($Re\leqslant 10$), the calculated Nusselt/Sherwood numbers are very close to the ones calculated under the assumption of Stokesian flow (their fractional difference is less than 10%). However, as Re increase, this difference deviates considerably and becomes more pronounced at the higher values of Pe. This observation would cast doubts on the applicability at high Re of any results obtained by computations using the Stokesian velocity profile.

4.4. Validation of numerical results

Acrivos and Taylor [8] derived asymptotic solutions that are applicable at the limit of creeping flow as well as at small but finite Re:

$$Nu=0.991Pe^{1/3}+0.922 \quad \text{and}$$
$$Nu=0.991Pe^{1/3}\left(1+\frac{1}{16}Re+\frac{3}{160}Re^2\ln Re+\mathrm{O}(Re^2)\right). \tag{25}$$

For the case of liquid sphere, Levich [2] also provided an asymptotic first-order solution for a liquid sphere at very large Pe under the condition of creeping flow

$$Nu=\left[\frac{4}{3\pi}\frac{1}{1+\lambda}Pe\right]^{1/2}. \tag{26}$$

In the case of a bubble ($\lambda=0$), we have found out that an exact correlation based on this asymptotic solution is: $Nu=0.651Pe^{1/2}+1.600$. The Nusselt/Sherwood numbers at low Re have been compared to these asymptotic solutions. The results are shown in Fig. 4. As observed in this figure, the results at $Re\to 0$ for both the bubble and the solid sphere agree very well with the solutions of Levich [2] and Acrivos and Taylor [8]. This validates the numerical method used in this study.

4.5. Correlations for Nu and Sh

Based on the numerical results, which are explicitly shown in Table 1, we have tried to develop working correlations for the Nusselt or Sherwood numbers as functions of Re, Pe and λ. These correlations of the results show the explicit influence of the viscosity ratio and are an improvement to similar correlations, which appear in the literature and are applicable to solid spheres or inviscid bubbles [20,21]. Because of the complexity of the problem, which is a result of the presence of three variables, we had to separate the ranges of validity of the correlations into several sub ranges:

A. At small but finite Re $(0<Re<1)$ and $Pe>10$, we are able to derive a general expression for Nu/Sh, which is as follows:

$$\begin{aligned}Nu(\lambda,Pe,Re)&=\left(\frac{0.651}{1+0.95\lambda}Pe^{1/2}+\frac{0.991\lambda}{1+\lambda}Pe^{1/3}\right)(1+\alpha(Re))\\&\quad+\left(\frac{1.65(1-\alpha(Re))}{1+0.95\lambda}+\frac{\lambda}{1+\lambda}\right),\end{aligned} \tag{27a}$$

where the function $\alpha(Re)$ is expressed as follows:

$$\alpha(Re)=\frac{0.61Re}{Re+21}+0.032. \tag{27b}$$

B. For higher Re the analysis of the data revealed that the best correlations (that is those that result in minimum standard deviation) are obtained when the general correlations for Nu or Sh are given in terms of the following three functions:

B1. The correlation for the Nu or Sh for an inviscid sphere ($\lambda=0$), which is as follows:

$$\begin{aligned}Nu(0,Pe,Re)&=0.651Pe^{1/2}\left(1.032+\frac{0.61Re}{Re+21}\right)\\&\quad+\left(1.60-\frac{0.61Re}{Re+21}\right).\end{aligned} \tag{28a}$$

B2. The corresponding function of Nu or Sh for a solid sphere ($\lambda=\infty$), which is as follows:

$$\begin{aligned}Nu(\infty,Pe,Re)&=0.852Pe^{1/3}\left(1+0.233Re^{0.287}\right)\\&\quad+1.3-0.182Re^{0.355}.\end{aligned} \tag{28b}$$

B3. The corresponding function of Nu or Sh for a sphere with viscosity ratio equal to 2 ($\lambda=2.0$), which is as follows:

Table 1
Nusselt/Sherwood numbers for a viscous sphere

$\lambda \setminus Pe$	1	10	20	50	100	200	500	1000
Stokes flow ($Re \to 0$)								
0	2.333	3.682	4.544	6.264	8.198	10.906	16.29	22.37
0.5	2.318	3.533	4.283	5.755	7.391	9.669	14.09	19.09
1	2.311	3.459	4.153	5.495	6.969	9.008	12.928	17.27
2	2.302	3.381	4.015	5.219	6.518	8.264	11.626	15.31
5	2.297	3.315	3.896	4.971	6.100	7.606	10.4	13.356
10	2.294	3.283	3.838	4.852	5.901	7.276	9.78	12.383
100	2.291	3.250	3.778	4.726	5.688	6.922	9.104	11.304
Solid	2.289	3.24	3.763	4.698	5.643	6.85	8.972	11.097
$Re = 1$								
0	2.354	3.778	4.681	6.482	8.482	11.336	16.986	23.349
0.5	2.341	3.628	4.419	5.967	7.686	10.078	14.741	20.0
1	2.334	3.553	4.285	5.699	7.251	9.396	13.509	18.12
2	2.326	3.472	4.141	5.41	6.779	8.65	12.226	16.1
5	2.322	3.404	4.016	5.147	6.335	7.919	10.860	13.964
10	2.319	3.371	3.955	5.020	6.122	7.566	10.197	12.931
100	2.316	3.335	3.891	4.886	5.893	7.186	9.471	11.773
Solid	2.315	3.330	3.883	4.869	5.865	7.139	9.381	11.628
$Re = 10$								
0	2.395	4.082	5.143	7.242	9.584	12.9	19.47	26.88
0.5	2.385	3.938	4.880	6.716	8.745	11.550	17.13	22.38
1	2.380	3.859	4.734	6.417	8.240	10.795	15.73	21.36
2	2.372	3.767	4.568	6.079	7.707	9.933	14.174	18.713
5	2.368	3.686	4.416	5.754	7.157	9.026	12.480	16.112
10	2.365	3.645	4.340	5.594	6.885	8.578	11.661	14.849
100	2.362	3.601	4.258	5.420	6.588	8.085	10.728	13.387
Solid	2.362	3.595	4.248	5.398	6.552	8.024	10.611	13.201
$Re = 20$								
0	2.404	4.196	5.33	7.575	10.09	13.630	20.65	28.54
0.5	2.395	4.061	5.08	7.063	9.26	12.320	18.34	25.1
1	2.39	3.98	4.93	6.775	8.74	11.500	16.88	22.89
2	2.385	3.895	4.769	6.412	8.181	10.596	15.183	20.276
5	2.379	3.8	4.592	6.036	7.546	9.560	13.31	17.263
10	2.376	3.756	4.508	5.857	7.24	9.052	12.358	15.8
100	2.373	3.708	4.417	5.660	6.902	8.487	11.228	14.094
Solid	2.373	3.702	4.405	5.636	6.8	8.417	11.149	13.878
$Re = 50$								
0	2.415	4.339	5.576	8.025	10.77	14.63	22.26	30.84
0.5	2.408	4.227	5.363	7.579	10.03	13.45	20.17	27.7
1	2.403	4.152	5.221	7.277	9.525	12.62	18.69	25.47
2	2.398	4.063	5.051	6.913	8.914	11.638	16.838	22.622
5	2.392	3.961	4.855	6.487	8.189	10.453	14.649	19.035
10	2.389	3.911	4.758	6.277	7.828	9.853	13.533	17.339
100	2.386	3.855	4.651	6.043	7.424	9.178	12.258	15.355
Solid	2.381	3.848	4.638	6.014	7.374	9.094	12.098	15.105
$Re = 100$								
0	2.423	4.431	5.736	8.321	11.223	15.307	23.374	32.441
0.5	2.417	4.341	5.564	7.958	10.604	14.307	21.579	29.726
1	2.413	4.275	5.438	7.688	10.141	13.471	19.562	25.499
2	2.406	4.181	5.262	7.317	9.53	12.539	18.326	24.746
5	2.401	4.077	5.060	6.871	8.761	11.260	15.798	20.358
10	2.398	4.021	4.952	6.635	8.360	10.608	14.660	18.756
100	2.394	3.959	4.831	6.278	7.756	9.630	12.936	16.268
Solid	2.384	3.951	4.815	6.243	7.695	9.529	12.743	15.946

(*continued on next page*)

Table 1 (*continued*)

$\lambda \setminus Pe$	1	10	20	50	100	200	500	1000
$Re = 200$								
0	2.424	4.482	5.835	8.539	11.578	15.851	24.285	33.759
0.5	2.420	4.416	5.708	8.259	11.109	15.078	22.865	31.578
1	2.417	4.364	5.607	8.043	10.726	14.444	21.695	29.778
2	2.412	4.287	5.458	7.713	10.157	13.481	19.84	27.06
5	2.405	4.168	5.232	7.223	9.243	12.021	17.262	22.937
10	2.391	4.042	5.019	6.815	8.472	10.816	15.122	19.67
100	2.386	3.974	4.889	6.412	8.002	10.045	13.648	17.283
Solid	2.385	3.967	4.874	6.378	7.952	9.951	13.466	16.987
$Re = 500$								
0	2.426	4.528	5.922	8.726	11.887	16.340	25.136	35.010
0.5	2.424	4.488	5.845	8.559	11.594	15.842	24.181	33.503
1	2.422	4.454	5.779	8.399	11.329	15.392	23.317	32.138
2	2.419	4.4	5.672	8.162	10.893	14.616	21.895	29.896
5	2.401	4.211	5.342	7.507	9.556	12.558	18.203	24.283
10	2.394	4.122	5.183	7.187	9.077	11.802	16.83	22.119
100	2.387	4.034	5.023	6.868	8.806	11.350	15.869	20.378
Solid	2.386	4.025	5.006	6.692	8.524	10.901	15.081	19.277

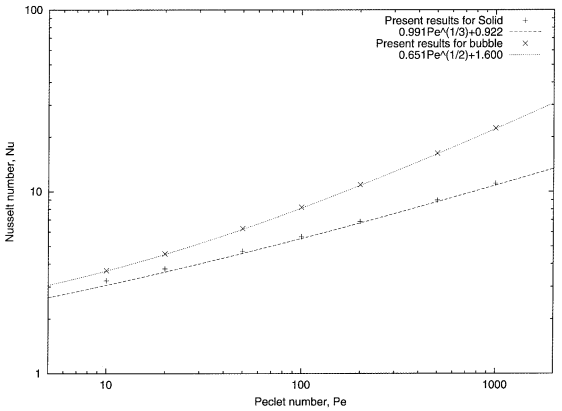

Fig. 4. Comparisons between numerical results and asymptotic solutions at creeping flow.

$$Nu(2, Pe, Re) = 0.64Pe^{0.43}\left(1 + 0.233Re^{0.287}\right) + 1.41 - 0.15Re^{0.287}. \quad (28c)$$

Thus, the final correlation functions obtained are given by the following expressions in the sub ranges $0 \leqslant \lambda < 2$ and $2 < \lambda \leqslant \infty$:

$$Nu(Pe, Re, \lambda) = \frac{2-\lambda}{2} Nu(Pe, Re, 0) + \frac{4\lambda}{6+\lambda} Nu(Pe, Re, 2) \quad \text{for } 0 \leqslant \lambda \leqslant 2, \text{ and } 10 \leqslant Pe \leqslant 1000 \quad (29a)$$

and

$$Nu(Pe, Re, \lambda) = \frac{4}{\lambda+2} Nu(Pe, Re, 2) + \frac{\lambda-2}{\lambda+2} Nu(Pe, Re, \infty) \quad \text{for } 2 \leqslant \lambda \leqslant \infty, \text{ and } 10 \leqslant Pe \leqslant 1000. \quad (29b)$$

As shown in the last two equations, these correlations are recommended for $Pe \geqslant 10$. At lower values of Pe, an interpolation of the values of Table 1 will yield more accurate results.

4.6. The effect of the density ratio

In our study on the hydrodynamic force exerted on a viscous sphere [17], we have found that, for a fixed value of Re and of the viscosity ratio, the variations of the density ratio, $\kappa = \rho_i/\rho_o$, have only a minimal effect on the external flow field. As a result, the drag coefficients are not sensitive to the density ratio κ. When one considers the mass/heat transfer equation (8) and the pertinent boundary condition (17), one will conclude that the density ratio (or equivalently

Table 2
The effect of the density ratio, κ, on the Nusselt/Sherwood numbers

$Re = 10.0, \lambda = 1.0$ $\kappa \setminus Pe$	1	10	20	50	100	200	500
0.1	2.38	3.858	4.734	6.418	8.241	10.796	15.732
1	2.38	3.859	4.734	6.417	8.240	10.795	15.730
10	2.38	3.857	4.732	6.414	8.235	10.789	15.726

the internal Reynolds number, Re_i) would not affect the Nusselt/Sherwood numbers. This was verified numerically by conducting computations with different values of the density ratio. The results of these computations are summarized in Table 2. It is apparent from this table that the results at different density ratios are almost identical. This supports the conclusion that the density ratio has almost no influence on the rate of heat or mass transfer from a viscous sphere.

5. A note on the deformation of the droplets at high Re

A central part of the applicability of the results in this paper is that at high values of Re the droplet remains spherical. Early experimental evidence by Winnikow and Chao [22] on the free fall or rise of drops in liquids shows that a liquid drop will remain spherical when the dimensionless Bond number, Bo, which is equal to the ratio We/Fr, is less than or equal to 0.2, that is when

$$Bo = \frac{We}{Fr} = \frac{g d_{eq}^2 |\rho_s - \rho_f|}{\sigma_{force}} \leqslant 0.2. \tag{30}$$

A closer look at the experimental data of the paper actually reveals that the eccentricity of the organic drops in water is below 5% at $Bo < 0.4$ and that the eccentricity of drops of several liquids (including water) in air is less than 5% at $Bo < 0.6$. Even in the most restricted case of this criterion ($Bo < 0.2$) calculations show that water droplets in air will maintain their spherical shape at values of Re up to 470. In the case of a substance with high surface tension the corresponding Re would be much larger (Re up to 1150 for mercury droplets). The experiments of Winnikow and Chao [22] also show that drops of m-nitrotoluene in water with $d = 3.1$ mm remain spherical at Re above 500. Therefore, the values of Re in this study are not too high for droplets to retain their spherical shape.

6. Conclusions

At high Re and Pe, momentum and thermal boundary layers are formed outside a viscous sphere. The use of two computational sub-domains for the external fields, allows us to compute accurately the velocity field and the temperature/concentration field outside the sphere. Hence, we are able to solve with a high degree of accuracy the governing equations and to determine the forces as well as the rates of heat and mass transfer from the viscous sphere. The numerical data obtained are presented here in terms of the Sherwood/Nusselt numbers in a tabular as well as in a correlation form, which may be used in engineering calculations. It is observed that Reynolds and Peclet numbers (or equivalently the Prandtl and Schmidt numbers) and the viscosity ratio play an important role on the rate of heat or mass transfer from the viscous sphere. On the contrary, the density ratio does not affect at all the Sherwood and Nusselt numbers.

Acknowledgements

This work was partially supported by grants from the NASA and Louisiana Education Quality Science Fund to Tulane University as well as by the Office of Naval Research to the Tulane-Xavier Center for Bioenvironmental Research (CBR), for which the authors are thankful.

References

[1] J. Fourier, Theorie Analytique de la Chaleur, Paris, 1822.
[2] V.G. Levich, Physicochemical Hydrodynamics, Prentice-Hall, Englewood Cliffs, NJ, 1962.
[3] S.L. Soo, Multiphase Fluid Dynamics, Science Press, Beijing, 1990.
[4] R. Clift, J.R. Grace, M.E. Weber, Bubbles, Drops and Particles, Academic Press, New York, 1978.
[5] G. Leal, Laminar Flow and Convective Transport Processes, Butterworth–Heineman, Boston, 1991.
[6] W.A. Sirignano, Fluid Dynamics and Transport of Droplets and Sprays, Cambridge University Press, Cambridge, 1999.
[7] S.K. Friedlander, Mass and heat transfer to single spheres and cylinders at low Reynolds numbers, AIChE J. 3 (1957) 43–48.
[8] A. Acrivos, T.E. Taylor, Heat and mass transfer from single spheres in Stokes flow, Phys. Fluids 5 (1962) 387–394.
[9] B. Abramzon, C. Elata, Heat transfer from a single sphere in Stokes flow, Int. J. Heat Mass Transfer 27 (1984) 687–695.
[10] Z.-G. Feng, E.E. Michaelides, A numerical study on the transient heat transfer from a sphere at high Reynolds and Peclet numbers, Int. J. Heat Mass Transfer 43 (2000) 219–229.
[11] Z.G. Feng, E.E. Michaelides, Mass and heat transfer form spheres at low Reynolds numbers, Powder Technology 112 (2000) 63–69.
[12] R.J. Haywood, N. Nafziger, M. Rengsibulut, A detailed examination of gas and liquid phase transient processes in convective droplet evaporation, J. Heat Transfer 111 (1989) 495–502.
[13] C.H. Chiang, M.S. Raju, W.A. Sirignano, Numerical analysis of convecting, vaporizing, fuel droplet with variable properties, Int. J. Heat Mass Transfer 35 (1992) 1307–1324.
[14] D. Hammerton, F.H. Garner, Mass transfer from bubbles, Trans. Int. Chem. Eng. 32 (Suppl.) (1954) S-18.
[15] Z.-G. Feng, E.E. Michaelides, Unsteady heat transfer from a spherical particle at finite Peclet numbers, J. Fluids Eng. 118 (1996) 96–102.

[16] C.W. Bowman, D.M. Ward, A.I. Johnson, O. Trans, Mass transfer from fluid and solid spheres at low Reynolds numbers, Can. J. Chem. Eng. (1961) 913.
[17] Z.G. Feng, E.E. Michaelides, The drag coefficients of a viscous sphere at intermediate and high Reynolds numbers, J. Fluids Eng. (in press).
[18] V.Y. Rivkind, G.M. Ryskin, G.A. Fishbein, Flow around a spherical drop in a fluid medium at intermediate Reynolds numbers, Appl. Math. Mech. 40 (1976) 687–691.
[19] M.A.I. El-Shaarawi, A. Al-Farayedhi, M.A. Antar, Boundary layer flow about and inside a liquid sphere, J. Fluids Eng. 119 (1997) 42–49.
[20] F.P. Incropera, D.P. De Witt, Fundamentals of Heat and Mass Transfer, Wiley, New York, 1985.
[21] M. Kaviany, Principles of Convective Heat Transfer, Springer, New York, 1994.
[22] S. Winnikow, B.T. Chao, Droplet motion in purified systems, Phys. Fluids 9 (1966) 50–61.